

This work was written as part of one of the author's official duties as an Employee of the United States Government and is therefore a work of the United States Government. In accordance with 17 U.S.C. 105, no copyright protection is available for such works under U.S. Law.

Public Domain Mark 1.0

<https://creativecommons.org/publicdomain/mark/1.0/>

Access to this work was provided by the University of Maryland, Baltimore County (UMBC) ScholarWorks@UMBC digital repository on the Maryland Shared Open Access (MD-SOAR) platform.

Please provide feedback

Please support the ScholarWorks@UMBC repository by emailing scholarworks-group@umbc.edu and telling us what having access to this work means to you and why it's important to you. Thank you.

Damping of acoustic vibrations in gold nanoparticles

Matthew Pelton^{1*}, John E. Sader², Julien Burgin^{3†}, Mingzhao Liu^{1,3†}, Philippe Guyot-Sionnest³ and David Gosztola¹

Studies of acoustic vibrations in nanometre-scale particles can provide fundamental insights into the mechanical properties of materials because it is possible to precisely characterize and control the crystallinity and geometry of such nanostructures^{1–4}. Metal nanoparticles are of particular interest because they allow the use of ultrafast laser pulses to generate and probe high-frequency acoustic vibrations, which have the potential to be used in a variety of sensing applications. So far, the decay of these vibrations has been dominated by dephasing due to variations in nanoparticle size⁵. Such inhomogeneities can be eliminated by performing measurements on single nanoparticles deposited on a substrate^{6–9}, but unknown interactions between the nanoparticles and the substrate make it difficult to interpret the results of such experiments. Here, we show that the effects of inhomogeneous damping can be reduced by using bipyramidal gold nanoparticles with highly uniform sizes¹⁰. The inferred homogeneous damping is due to the combination of damping intrinsic to the nanoparticles and the surrounding solvent; the latter is quantitatively described by a parameter-free model.

As well as basic studies of material properties, resonant vibrations in nanostructures enable a range of applications, including molecular-scale biological sensing and ultrasensitive mass detection^{11–14}. To approach the ultimate limit of single atom sensing, it is necessary to reduce the dimensions of the structures to the nanoscale while keeping the damping of the vibrations as low as possible. Ultrafast laser spectroscopy allows for the direct time-domain study of vibration frequencies and damping rates in metal nanoparticles^{5,15,16}, complementing frequency-domain techniques such as Brillouin scattering³ and Raman scattering⁴. Light from a pump laser pulse is absorbed by conduction electrons in the metal, which immediately transfer their excess energy to the lattice, causing the nanoparticle to expand. This rapid expansion corresponds to nearly impulsive excitation of the acoustic vibrations. As the particles vibrate, the frequencies of plasmon resonances in the nanoparticles are modulated. Extinction of a second laser pulse tuned near a plasmon resonance can thus serve as a sensitive probe of the vibrations.

Development of applications requires an understanding of the damping inherent to the nanoparticles themselves and damping due to energy transfer to the fluid surroundings. Here, we tackle both these outstanding issues by measuring and modelling a highly monodisperse colloidal nanoparticle system. We chemically synthesized bipyramidal gold nanoparticles in solution using a seed-mediated growth technique¹⁰. The resulting particles have particularly low variance in their dimensions, as determined from

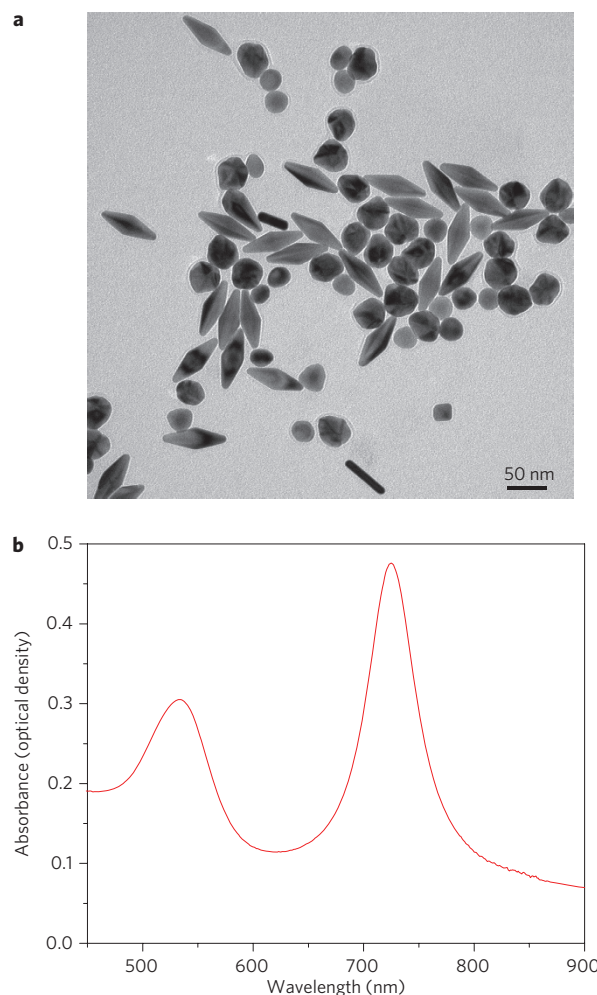


Figure 1 | Chemically synthesized bipyramidal gold nanoparticles.

a, TEM image of nanoparticles as synthesized. **b**, Linear extinction spectrum of nanoparticles, capped with polystyrene sulphonic acid (PSS), in water.

transmission electron microscope (TEM) images such as that in Fig. 1a. The monodispersity is also manifest in the linear absorption spectrum (Fig. 1b). The strong peak at 725 nm (1.7 eV) is due to the longitudinal plasmon resonance in the bipyramids, corresponding to coherent oscillation of conduction electrons along the long axes

¹Center for Nanoscale Materials, Argonne National Laboratory, Argonne, Illinois 60439, USA, ²Department of Mathematics and Statistics, The University of Melbourne, Victoria 3010, Australia, ³James Franck Institute, The University of Chicago, Chicago, Illinois 60637, USA; [†]Present address: ICMCB, CNRS and Université de Bordeaux, 87, Avenue du Docteur Albert Schweitzer, 33608 PESSAC, France (J.B.); Department of Chemistry and Chemical Biology, Harvard University, Cambridge, Massachusetts 02143, USA (M.L.). *e-mail: pelton@anl.gov

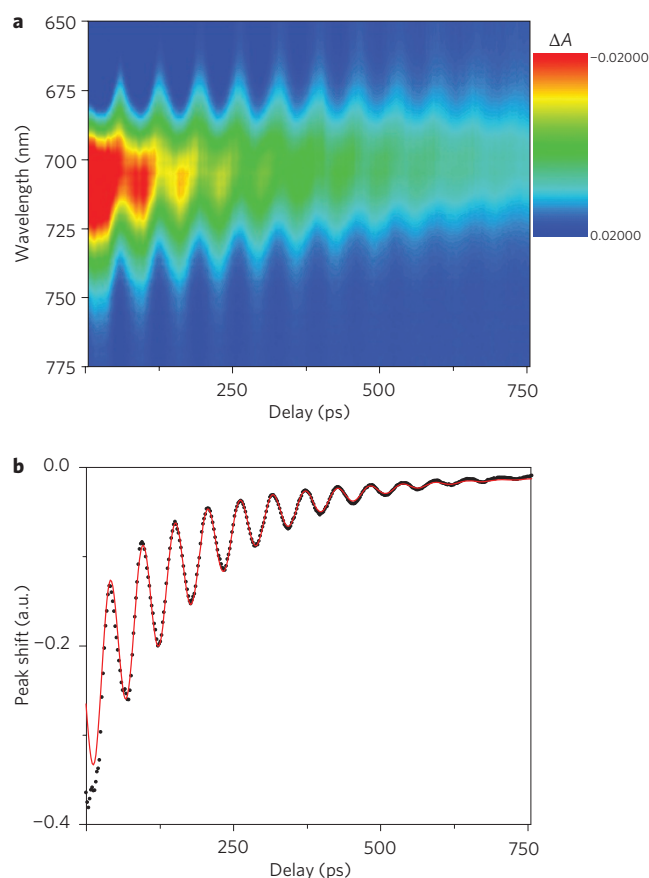


Figure 2 | Transient spectroscopy of gold nanoparticles. **a**, Colour map of transient extinction from the sample shown in Fig. 1 (bipyramidal gold nanoparticles, capped with PSS, in water), following excitation by a pump laser pulse with a wavelength of 725 nm and an energy of 100 nJ. ΔA is defined in the Methods. **b**, Change in the peak frequency of the longitudinal plasmon resonance in bipyramidal gold nanoparticles. Points: measurement results obtained by fitting the experimental data in **a**. Line: fit, including homogeneous and inhomogeneous damping, according to equation (1).

of the particles¹⁰. The narrow linewidth of this peak (130 meV) reflects low inhomogeneous broadening due to small variations in particle shape, as well as low homogeneous broadening (~ 95 meV)¹⁰ due to the weak optical absorption of gold at this wavelength. The broader peak at ~ 525 nm is primarily due to the presence of an irregular, spheroidal byproduct (Fig. 1a). Because the two peaks are well separated spectrally, the response of the bipyramids can be isolated by probing only at wavelengths around 725 nm.

The acoustic vibrations were measured by exciting the sample with an ultrafast pump laser pulse and, after a controlled delay, measuring the extinction of a probe pulse. Data were collected as a function of the pump–probe delay time and of the probe wavelength (Fig. 2a). The measured changes in probe extinction are due to broadening and shifting of the longitudinal plasmon peak⁵; the peak shift was determined by fitting the transient spectra (see Supplementary Information). The fitted peak shift (Fig. 2b) shows pronounced oscillations resulting from acoustic vibrations⁵ on top of an exponentially decaying background that is due to gradual cooling of the gold lattice¹. The signal due to the vibrations is well separated from the electronic response of the nanoparticles, which occurs on timescales of less than 10 ps.

The observed decay of the vibrations is a combination of inhomogeneous dephasing due to the variation in particle sizes and homogeneous damping due to energy loss. To estimate

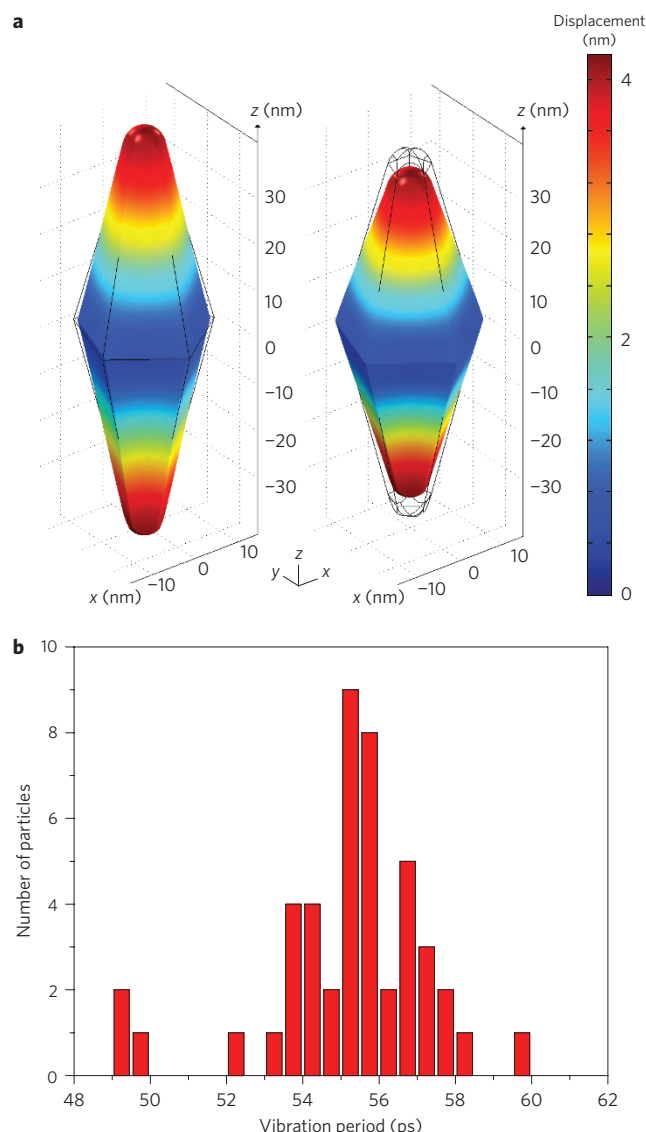


Figure 3 | Simulation of acoustic vibrations in gold nanoparticles.

a, Displacement associated with the lowest-frequency symmetric vibrational mode. The thin lines represent the boundaries of the particle at rest and the colour scale corresponds to the total magnitude of displacement. The left-hand and right-hand panels correspond to the maximum and minimum displacements, respectively. Because the simulations were used to determine only the vibrational frequency of the mode, the overall magnitude of the oscillations is arbitrary and is much larger than in the experiments. The particle shown has a length of 78.7 nm, a diameter of 28.4 nm and rounded tips with a radius of curvature of 5 nm, corresponding to the mean particle dimensions measured by TEM. **b**, Histogram of calculated vibrational periods, for nanoparticles for which the dimensions were measured from electron microscope images.

the degree of inhomogeneous dephasing, we used finite-element simulations of the acoustic vibrations, as illustrated in Fig. 3a. The simulation was repeated for 52 bipyramids with different lengths and diameters, corresponding to the dimensions of individual nanoparticles as determined from TEM images (see Supplementary Information for details). Previous TEM measurements have shown that the bipyramids all have the same crystal structure and are nearly free of defects, apart from five twinning planes running along their long axes¹⁰; it is therefore expected that the particles have identical mechanical properties, so that variation in nanoparticle shape is the only factor contributing to variation in the vibrational period.

Table 1 | Homogeneous damping times, resonant frequencies and quality factors for acoustic vibrations in a sample of bipyramidal gold nanoparticles, capped with PSS, for different solvents.

Solvent	Measured homogeneous damping time, T_1 (ps)	Resonant frequency, f (GHz)		Q_1		Q_{fluid}
		Measurement	Theory	Measurement	Theory	Theory
Methanol	286 ± 40	19.2 ± 0.1	19.8	17.3 ± 2.4	17.5 ± 1.5	58.6 ± 2.2
Water	261 ± 10	19.1 ± 0.3	19.8	15.7 ± 0.6	15.5 ± 1.2	41 ± 3
Ethylene glycol	137 ± 12	20.0 ± 0.6	18.9	8.6 ± 0.8	7.1 ± 0.2	9.9 ± 0.5
Glycerol	28 ± 10	18 ± 2	(13.8)	1.6 ± 0.6	(1.9 ± 0.1)	(2.1 ± 0.1)

Theoretical values of total homogeneous quality factors, Q_1 , are determined using the quality factors, Q_{fluid} , calculated using the parameter-free model for viscous damping by the solvent and an intrinsic quality factor $Q_{\text{intrinsic}} = 25 \pm 3$. Theoretical results for glycerol are in parentheses because the model is not applicable to that system.

As shown in Fig. 3b, the periods are well described by a normal distribution with an average of $T_0 = 55 \pm 3$ ps and a standard deviation of $\sigma_T = 2.1 \pm 0.1$ ps. Because σ_T is small compared to T_0 , the inhomogeneous dephasing time is¹⁷ $T_2^* \approx T_0^2/(\sqrt{2\pi}\sigma_T) = 327 \pm 33$ ps.

Using this estimate for the inhomogeneous dephasing time, we fit the measured time-dependent peak shift for delays from 75 to 750 ps to the following formula¹⁷:

$$\Delta\Omega(t) = A_0 \exp\left(-\frac{t}{T_1}\right) \exp\left(-\frac{t^2}{(T_2^*)^2}\right) \sin\left(\frac{2\pi t}{T} + \phi\right) + A_1 \exp\left(-\frac{t}{\tau_{\text{cool}}}\right) \quad (1)$$

where T is the period of acoustic vibrations, T_1 their homogeneous damping time, τ_{cool} the time for heat exchange between the nanoparticle and the surrounding solvent, ϕ a phase factor, and A_0 and A_1 proportionality constants. The result of a representative fit is shown in Fig. 2b. The fitted values of T_1 were observed to be largely independent of pump wavelength but dependent on the pump-pulse energy. The cause of this dependence is not entirely clear, but it may be that an increase in pump power leads to an increase in the local temperature of the solvent around the nanoparticles; this would lower the viscosity of the solvent, resulting in weaker damping of the oscillations. To remove this power-dependent effect, we performed a linear regression on the fitted values of T_1 and extrapolated to zero pump power.

The entire measurement and fitting process was repeated on the same sample after it was transferred from water to several other solvents. Fitted values for the homogeneous damping time, T_1 , are given in Table 1 (with error estimates based on statistical error in the calculated value of T_2^*). Also shown are homogeneous quality factors, $Q_1 = \pi f T_1$, where the vibrational resonance frequency is $f = 1/[T\sqrt{1 - (1/4Q_1^2)}]$. The homogeneous damping time can be seen to change significantly when the particles are transferred from one solvent to another.

Having removed the effect of inhomogeneous dephasing, we can further subdivide the homogeneous damping into two parts: viscous damping by the surrounding fluid and solvent-independent processes intrinsic to the nanoparticles themselves; that is, $1/Q_1 = 1/Q_{\text{fluid}} + 1/Q_{\text{intrinsic}}$. We theoretically modelled the fluid damping by approximating the bipyramid as a narrow rod oscillating in a viscous fluid^{18,19} (see Supplementary Information for details). The calculated resonance frequency and quality factor are $f = f_{\text{vac}}/\sqrt{1 + \Gamma(f)}$ and $Q_{\text{fluid}} = 1 + 1/\Gamma(f)$, respectively, where

$$\Gamma = 2.44(1 - 4.05[1 - L/L_T]^2) \frac{1}{\rho_s} \sqrt{\frac{\mu\rho}{\pi f R^2}} \quad (2)$$

where f_{vac} is the resonance frequency in vacuum, L the length of the particle, L_T its projected length (see Supplementary Fig. S1), ρ the

density of the fluid, ρ_s the density of gold, R the maximum radius of the particle and μ the fluid shear viscosity. The model is derived in the limit of high inertia, where the viscous boundary layer surrounding the particle is assumed to be thin. This assumption is valid for the lower-viscosity solvents investigated (methanol, water and ethylene glycol), but not for glycerol, where the boundary-layer thickness significantly exceeds the particle width (see Supplementary Table S1).

Resonance frequencies and quality factors due to the fluid can thus be calculated without any adjustable parameters (see results in Table 1). We can then take the intrinsic quality factor as the single adjustable parameter to calculate theoretical homogeneous quality factors, Q_1 . As shown in Table 1, $Q_{\text{intrinsic}} = 25 \pm 3$ gives good agreement between theory and experiment for all three lower-viscosity solvents. Note that this value relies primarily on the measurement results in water and methanol; for particles in ethylene glycol, the homogeneous damping is dominated by the fluid. Note also that the accuracy of this value for $Q_{\text{intrinsic}}$ depends on the accuracy of the model for fluid damping and of the model used to calculate the inhomogeneous damping time T_2^* . If, for example, there are additional contributions to T_2^* due to hidden structural inhomogeneities, then the true value of $Q_{\text{intrinsic}}$ will be greater.

The intrinsic damping has contributions due to mechanisms occurring in the gold cores of the nanoparticles and in the surface layer of organic molecules. By making measurements on a second sample with a series of different capping molecules (see Supplementary Information), we estimate that the capping molecules may be responsible for up to 26% of the intrinsic damping. The intrinsic quality factor we infer is comparable to quality factors measured for single metal particles on solid substrates: $Q_1 = \pi f T_1 = 15$ –30 for breathing modes in gold nanospheres⁶, 7–12 for silver nanocubes^{7,8}, 12 ± 3 for silver nanowires⁸ and 37 ± 6 for extensional modes in gold nanorods⁹. In these previous systems, however, the mechanical coupling of the particles to the substrates is unknown.

The intrinsic quality factor we measure for bipyramidal gold nanoparticles is about two orders of magnitude smaller than the highest reported quality factors for vibrations in microscopic silicon cantilevers¹¹, an order of magnitude lower than the highest values for carbon nanotubes¹³, and comparable to values for single graphene sheets¹². The reduced quality factor compared to semiconductor structures is most likely due to stronger inherent damping mechanisms in metals²⁰. Improvements in the synthesis of nanoparticles with reduced size variations will allow our technique to be applied to particles made of materials with lower mechanical losses, making it possible to measure vibrations with very high frequencies (in the range 10–100 GHz) and high quality factors. The use of optical sensing techniques makes it possible to avoid noise and bandwidth limitations associated with electronic measurements at these frequencies. This will have far-reaching implications for the development of nanomechanical devices such as ultrasensitive chemical sensors operating in fluid.

Methods

Nanoparticle synthesis. Bipyramidal gold nanoparticles were prepared using a seed-mediated growth process¹⁰. Spherical gold seed nanoparticles were first produced by adding, with vigorous stirring at room temperature, 0.3 ml of freshly prepared 10 mM NaBH₄ aqueous solution to an aqueous solution containing 20 ml of 0.125 mM HAuCl₄ and 0.25 mM sodium citrate. Following aging for at least 2 h, 80 µl of this sol was injected into an aqueous growth solution prepared as follows: 0.5 ml of 10 mM HAuCl₄ and 0.08 ml of 10 mM AgNO₃ were mixed with 10 ml of 0.1 M cetyltrimethylammonium bromide (CTAB), the solution acidified with 0.2 ml of 1.0 M HCl to a pH between 3 and 4, and the Au(III) reduced to Au(I) by the addition of 0.08 ml of 0.1 M L-ascorbic acid. The growth reaction was performed at 30 °C under gentle stirring for ~2 h.

As grown, the nanoparticles are capped with a bilayer of CTAB. This layer could be exchanged with polystyrene sulphonic acid (PSS), a negatively charged polymer, as follows. First, the solution was cooled to 5 °C for several hours, causing excess CTAB to precipitate in crystalline form. This precipitate was removed by centrifugation at 2,000g before the solution was brought back to room temperature. The gold nanoparticles were then precipitated by centrifugation at 7,000g for 6 min. The precipitate was dissolved in a 0.1% aqueous solution of PSS, and the solution left to stand for at least 1 h at room temperature, so that the PSS adsorbed onto the surfaces of the nanoparticles. The solution was then centrifuged again at 7,000g and the supernatant was discarded. The resulting PSS-capped nanoparticles could be dissolved into a variety of solvents, including water, methanol, ethylene glycol and glycerol. Alternatively, the particles could be coated with hexanethiol or dodecanethiol. To achieve this, 20 µl of 10 mM thiol solution in ethanol was added to 1 ml aqueous solution of CTAB-coated bipyramids. The solution was agitated, and excess CTAB was removed as described above.

Transient-extinction spectroscopy. Time-resolved measurements were performed with a commercial transient spectrometer (Newport Helios). Pump and probe pulses were derived from a regeneratively amplified Ti:sapphire laser (Newport Tsunami and SpitFire Pro), which produced 120-fs pulses at 5 kHz. Ninety percent of the amplified laser pulse was used to pump an optical parametric amplifier (OPA; Newport TOPAS-C). The output pulses from the OPA were also ~120 fs in duration and served as the pump pulses. The remainder of the amplified beam passed down a variable-delay line and was focused into a sapphire crystal, generating a continuum probe pulse. The continuum was passed through an interference notch filter (Semrock NF01-808U-25) to remove residual light at the fundamental wavelength of 800 nm, and the filtered probe pulse was focused onto the sample. The pump pulse was focused to an overlapping spot on the sample after passing through a variable neutral-density filter to control its power; the beam diameter at the focus was ~550 µm for a wavelength of 750 nm. The sample was held in a 2-mm quartz cuvette and stirred continually during measurement. After passing through the sample, the probe pulse was detected using a fibre-coupled spectrometer, equipped with a CCD detector, which measured the complete spectrum of the probe pulse in a single shot. The pump pulse was modulated with a mechanical chopper, synchronized with the regenerative amplifier, at 2.5 kHz, so that the spectrometer alternately measured the probe transmittance, T_{on} and T_{off} , in the presence and in the absence of the pump pulse, respectively. The differential extinction $\Delta A = -\log_{10}(T_{\text{on}}/T_{\text{off}})$ was calculated for each pair of pulses and was averaged over several thousand shots for each time delay between pump and probe. Background signal due to scattered pump light was removed by averaging approximately 10 spectra at negative pump–probe delays and subtracting the result from all subsequent spectra. Temporal chirp in the probe pulse was determined by making a measurement on neat solvent; the resonant signal was fitted for each probe wavelength to determine the zero-delay position between pump and probe, and experimental data were corrected accordingly.

For each sample, measurements were performed (i) for a pump wavelength at the maximum of the longitudinal plasmon resonance (resonant measurements) and (ii) for a pump wavelength between 375 and 450 nm (non-resonant measurements). The resulting vibrational decay times are very similar in the two cases, reflecting the small size dispersion in the sample. Measurements reported in the main text are for pump wavelengths resonant with the longitudinal plasmon resonance.

Measurements were performed for pump pulse energies of 20, 50 and 100 nJ. For each measurement, the pump–probe delay scan was repeated twice and the two scans averaged to give the final result. Linear extinction spectra were measured before and after the transient measurements to ensure that the samples were not damaged by the laser powers used.

Received 20 April 2009; accepted 22 June 2009;
published online 26 July 2009

References

- Hartland, G. V. Measurements of the material properties of metal nanoparticles by time-resolved spectroscopy. *Phys. Chem. Chem. Phys.* **6**, 5263–5274 (2004).
- Tang, Y. & Ouyang, M. Tailoring properties and functionalities of metal nanoparticles through crystallinity engineering. *Nature Mater.* **6**, 754–759 (2007).
- Still, T. *et al.* The ‘music’ of core–shell spheres and hollow capsules: influence of the architecture on the mechanical properties at the nanoscale. *Nano Lett.* **8**, 3194–3199 (2008).
- Portales, H. *et al.* Probing atomic ordering and multiple twinning in metal nanocrystals through their vibrations. *Proc. Natl Acad. Sci. USA* **105**, 14784–14789 (2008).
- Hartland, G. V. Coherent excitation of vibrational modes in metallic nanoparticles. *Annu. Rev. Phys. Chem.* **57**, 403–430 (2006).
- van Dijk, M. A., Lippitz, M. & Orrit, M. Detection of acoustic oscillations of single gold nanospheres by time-resolved interferometry. *Phys. Rev. Lett.* **95**, 267406 (2005).
- Staleva, H. & Hartland, G. V. Transient absorption studies of single silver nanocubes. *J. Phys. Chem. C* **112**, 7535–7539 (2005).
- Staleva, H. & Hartland, G. V. Vibrational dynamics of silver nanocubes and nanowires studied by single-particle transient absorption spectroscopy. *Adv. Func. Mater.* **18**, 3809–3817 (2008).
- Zijlstra, P., Tchegobotava, A., Chon, J., Gu, M. & Orrit, M. Acoustic oscillations and elastic moduli of single gold nanorods. *Nano Lett.* **8**, 3493–3497 (2008).
- Liu, M. Z. & Guyot-Sionnest, P. Mechanism of silver(I)-assisted growth of gold nanorods and bipyramids. *J. Phys. Chem. B* **109**, 22192–22200 (2005).
- Yang, Y. T., Callegari, C., Feng, X. L., Ekinci, K. L. & Roukes, M. L. Zeptogram-scale nanomechanical mass sensing. *Nano Lett.* **6**, 583–586 (2006).
- Bunch, J. S. *et al.* Electromechanical resonators from graphene sheets. *Science* **315**, 490–493 (2007).
- Jensen, K., Kim, K. & Zettl, A. An atomic-resolution nanomechanical mass sensor. *Nature Nanotech.* **3**, 533–537 (2008).
- Burg, T. P. *et al.* Weighing of biomolecules, single cells and single nanoparticles in fluid. *Nature* **446**, 1066–1069 (2007).
- Del Fatti, N., Voisin, C., Christofilos, D., Vallée, F. & Flytzanis, C. Acoustic vibration of metal films and nanoparticles. *J. Phys. Chem. A* **104**, 4321–4326 (2000).
- Pelton, M., Aizpurua, J. & Bryant, G. W. Metal–nanoparticle plasmonics. *Laser Photon. Rev.* **2**, 135–169 (2008).
- Hartland, G. V. Coherent vibrational motion in metal particles: determination of the vibrational amplitude and excitation mechanism. *J. Chem. Phys.* **116**, 8048–8055 (2002).
- Sader, J. E. Frequency response of cantilever beams immersed in viscous fluids with applications to the atomic force microscope. *J. Appl. Phys.* **84**, 64–76 (1998).
- Saviot, L., Netting, C. & Murray, D. Damping by bulk and shear viscosity of confined acoustic phonons from nanostructures in aqueous solution. *J. Phys. Chem. B* **111**, 7457–7461 (2007).
- Nowick, A. S. & Berry, B. S. *Anelastic Relaxation in Crystalline Solids* (Academic Press, 1972).

Acknowledgements

Work at the Center for Nanoscale Materials was supported by the US Department of Energy (contract no. DE-AC02-06CH11357). J.B. was fully supported and M.Z.L. was partially supported by the US National Science Foundation (grant no. CHE-0718718). J.E.S. acknowledges support from the Australian Research Council Grants Scheme.

Author contributions

M.P. designed the research project, carried out the transient-absorption measurements, analysed the data and wrote the paper. J.E.S. developed the analytical model for fluid damping of nanoparticle vibrations and analysed the experimental results. J.B. carried out the finite-element modelling and contributed to data analysis. M.L. and J.B. synthesized the gold bipyramids and prepared the samples. P.G.S. contributed to project design and the understanding of the experimental results, and D.G. contributed to the transient-absorption measurement capabilities. All authors discussed the results and contributed to writing of the manuscript.

Additional information

Supplementary information accompanies this paper at www.nature.com/naturenanotechnology. Reprints and permission information is available online at <http://npg.nature.com/reprintsandpermissions/>. Correspondence and requests for materials should be addressed to M.P.